IEICE TRANS. COMMUN., VOL.E102–B, NO.2 FEBRUARY 2019

INVITED PAPER *Special Section on Recent Progress in Antennas and Propagation in Conjunction with Main Topics of ISAP2017*

Metasurface Antennas: Design and Performance

Marco FAENZI[†a)], **Gabriele MINATTI**[††], ***and*** **Stefano MACI**[†], ***Nonmembers***

SUMMARY This paper gives an overview on the design process of modulated metasurface (MTS) antennas and focus on their performance in terms of efficiency and bandwidth. The basic concept behind MTS antennas is that the MTS imposes the impedance boundary conditions (IBCs) seen by a surface wave (SW) propagating on it. The MTS having a spatially modulated equivalent impedance transforms the SW into a leaky wave with controlled amplitude, phase and polarization. MTS antennas are hence highly customizable in terms of performances by simply changing the IBCs imposed by the MTS, without affecting the overall structure. The MTS can be configured for high gain (high aperture efficiency) with moderate bandwidth, for wide bandwidth with moderate aperture efficiency, or for a trade-off performance for bandwidth and aperture efficiency. The design process herein described relies on a generalized form of the Floquet wave theorem adiabatically applied to curvilinear locally periodic IBCs. Several technological solutions can be adopted to implement the IBCs defined by the synthesis process, from sub-wavelength patches printed on a grounded slab at microwave frequencies, to a bed of nails structure for millimeter waves: in any case, the resulting device has light weight and a low profile.

key words: *metasurface antennas, leaky waves, artificial surfaces, Floquet waves, impedance boundary conditions*

1. Introduction

Metasurfaces (MTSs), the 2D equivalent of metamaterials, are thin artificial layers characterized by unusual reflection and transmission properties of plane waves and/or dispersion properties of surface/guided waves. At microwave frequencies, MTSs are implemented by printing sub-wavelength patches on a grounded dielectric substrate to realize homogenised impedance boundary conditions (IBCs).

The control of leaky wave (LW) radiation through the modulation of IBCs has led to a new class of antennas which sometimes are referred to as modulated MTS antennas [1]. This kind of antennas works on the transformation of a bounded SW into a radiative LW through the SW interaction with the MTS. Although modulated MTS antennas are based on a LW mechanism, their behaviour offers an enormous flexibility with respect to conventional LW antennas: due to the 2D control of the propagation and leakage parameters, it is possible to control phase and amplitude of the aperture field, and hence beam shape and polarization, efficiency and radiation pattern bandwidth. The ease with which the beam can be shaped is one of the most interesting features of MTS antennas, especially for peculiar fields as space applications. In this paper, however, we focus on the performance in terms of gain and bandwidth, being such parameters of general interest in a wider range of antenna applications.

At microwaves, MTS antennas are typically constituted by thousands of subwavelength patches of different shapes or metallic strips, printed on a grounded dielectric substrate [1]–[5]. For some millimeter and submillimeter wave applications, patch textures can be conveniently replaced by metallized pins textures [6]. Provided the elements implementing the IBCs are small in terms of the wavelength (between one fifth and one tenth of the wavelength), the interacting SW sees the texture as a continuum. The elements of the texture behave like pixels in a black&white printed image, whose grey scale is realized by changing the dimension of the pixel-elements inside a regular lattice.

MTS antennas exhibit low profile, low weight, reduced complexity, and low cost. No external protruding, backing feed arrangements or (sub-) reflectors are required: indeed, the feeding structure is embedded in the MTS plane. This is an advantage with respect to other types of printed antennas, like reflectarrays, especially for space applications [1].

In this paper, we review the analysis and design process of modulated MTS antennas, providing an overview of the performance that can be achieved in terms of gain and bandwidth. The paper is structured as follows: Section 2 introduces the adiabatic Floquet wave (FW) model for curvilinear locally periodic IBCs which is the basis for the design process described in the next Sect. 3 in a global frame, from the synthesis of the IBCs to the final antenna layout. Right after, Sects. 4 and 5 discuss efficiency and bandwidth of MTS antennas, respectively, with focus on broadside, circularly polarized beams. Concluding remarks are in Sect. 6.

2. Adiabatic Floquet Waves for Curvilinear IBCs

The adiabatic FW expansion is a theoretical model describing currents and fields on locally periodic IBCs, as the ones formed by the patch texture in MTS antennas.

The model, denoted as "Flat Optics" (FO) in [7], [8], is founded on the rigorous FW expansion of 1D periodic problems asymptotically extended to the case of locally periodic 2D IBCs. Even if the actual IBCs are not strictly periodic, the FW expansion still gives a good description of fields and

Manuscript received March 4, 2018.
Manuscript revised May 15, 2018.
Manuscript publicized August 21, 2018.

[†]The authors are with Department of Information Engineering and Mathematics, University of Siena, Via Roma 56, 53100, Siena, Italy.
[††]The author is with Wave Up S.r.l., Via Roma 77, 53100, Siena, Italy.
a) E-mail: faenzi@diism.unisi.it

DOI: 10.1587/transcom.2018ISI0004

Copyright © 2019 The Institute of Electronics, Information and Communication Engineers

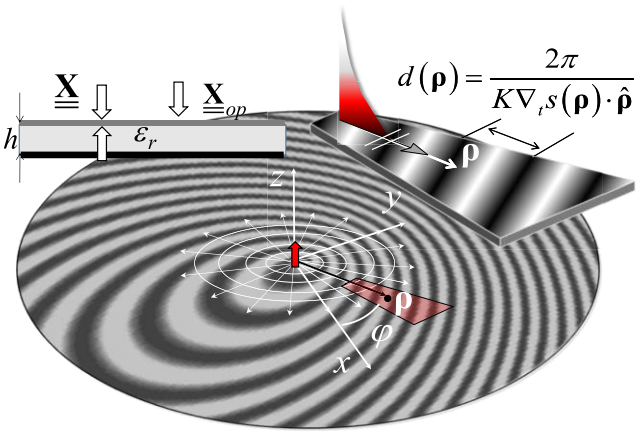

Fig. 1 Geometry of the problem. The subwavelength printed patches are modelled by an anisotropic tensor reactance, which defines through (1) a "transparent" IBC on a grounded dielectric slab (inset on the left corner). The inset on the right sketches the local periodic problem for the definition of the adiabatic Floquet modes.

currents associated with the local periodicity of the surface, and can be successfully exploited to design MTS antennas.

The FO model refers to MTSs consisting of a lossless grounded dielectric slab of relative permittivity ε_r and thickness h, printed with perfectly electric conducting subwavelength patches, constituting a penetrable IBC with modulated capacitive reactance. The reference configuration is shown in Fig. 1. The MTS is defined on a circular surface of radius a, centered at the origin of a cylindrical reference system with coordinates (ρ, φ) and unit vectors $(\hat{\boldsymbol{\rho}}, \hat{\boldsymbol{\varphi}})$. Bold characters denote vectors, bold characters underlined by a double bar denote tensors. At the interface between metal cladding and free space, the observation point is indicated by $\boldsymbol{\rho} = \rho\cos\varphi\hat{\mathbf{x}} + \rho\sin\varphi\hat{\mathbf{y}}$. Transverse magnetic (TM) and transverse electric (TE) modes are referred to the normal $\hat{\mathbf{z}}$ to the surface. Free-space wavenumber, wavelength and impedance are identified respectively by k, λ and ζ. The SW is assumed excited by a vertical electric dipole at the center of the reference system. The validity of this assumption relies in that, although the feed structure can be more complex than a dipole, the excited SW still has azimuthal symmetry, as the one launched by a vertical dipole.

Constant average non-uniform IBCs

We model the metallic cladding constituting the MTS with an anisotropic "transparent" IBC ([7], [9]) identified by

$$\mathbf{E}_t = j\underline{\underline{\mathbf{X}}}\cdot\hat{\mathbf{z}}\times(\mathbf{H}_t|_{0^+} - \mathbf{H}_t|_{0^-}) = j\underline{\underline{\mathbf{X}}}\cdot\mathbf{J} \tag{1}$$

where $\underline{\underline{\mathbf{X}}}$ is the penetrable or "transparent" reactance and $\mathbf{J}$ is the electric current flowing in the metallic homogenized cladding. In absence of losses, $\underline{\underline{\mathbf{X}}}$ is an Hermitian tensor [10] (analogously, the *impedance* $j\underline{\underline{\mathbf{X}}}$ is anti-Hermitian); the class of transparent *lossless* reactance tensors of our interest is referred to as "constant-average non uniform reactances", and is given by

$$\underline{\underline{\mathbf{X}}} = \underline{\underline{\mathbf{X}}}^{(0)} + \underline{\underline{\mathbf{X}}}^{(-1)} + \underline{\underline{\mathbf{X}}}^{(+1)} \tag{2}$$

$$\underline{\underline{\mathbf{X}}}^{(0)} = \overline{X}_\rho\hat{\boldsymbol{\rho}}\hat{\boldsymbol{\rho}} + \overline{X}_\varphi\hat{\boldsymbol{\varphi}}\hat{\boldsymbol{\varphi}} \tag{3}$$

$$\underline{\underline{\mathbf{X}}}^{(\mp1)} = \frac{1}{2}e^{\pm jKs(\boldsymbol{\rho})}\left[m_\rho(\boldsymbol{\rho})\left(\overline{X}_\rho\hat{\boldsymbol{\rho}}\hat{\boldsymbol{\rho}} - \overline{X}_\varphi\hat{\boldsymbol{\varphi}}\hat{\boldsymbol{\varphi}}\right)e^{\pm j\Phi_\rho(\boldsymbol{\rho})} + m_\varphi(\boldsymbol{\rho})\overline{X}_\rho\left(\hat{\boldsymbol{\rho}}\hat{\boldsymbol{\varphi}} + \hat{\boldsymbol{\varphi}}\hat{\boldsymbol{\rho}}\right)e^{\pm j\Phi_\varphi(\boldsymbol{\rho})}\right] \tag{4}$$

where $\overline{X}_\rho$ and $\overline{X}_\varphi$ are negative (capacitive), space independent quantities, K is a large ρ-independent constant such that $K|\nabla_t s(\boldsymbol{\rho})| \gg \left|\nabla_t\Phi_{\rho,\varphi}(\boldsymbol{\rho})\right|$, with the transverse gradient operating in $\boldsymbol{\rho}$, and $s(\boldsymbol{\rho})$ has unit peak value. We note that the symmetric tensors in (2)–(4) are representative of MTSs constituted by elements with two orthogonal symmetry axes and identify reactances with principal axes aligned with $(\hat{\boldsymbol{\rho}}, \hat{\boldsymbol{\varphi}})$. Also, (2)–(4) have a rapidly oscillating part described by $\underline{\underline{\mathbf{X}}}^{(\mp1)}$ that can be written in terms of cosine functions by combining together the exponential functions. Within the entries of $\underline{\underline{\mathbf{X}}}^{(\mp1)}$ one can identify three factors: (*i*) a rapidly varying phase factor $\exp(\pm jKs(\boldsymbol{\rho}))$, providing the main interaction with the exciting SW; (*ii*) the slowly varying phase factors $\exp\left(\pm j\Phi_{\rho,\varphi}(\boldsymbol{\rho})\right)$, which mainly control the polarization; (*iii*) the modulation indexes $m_{\varphi,\rho}(\boldsymbol{\rho})$, which mostly control the amplitude field. The condition $m_{\rho,\varphi}(\boldsymbol{\rho}) < 1$ avoids local changes of the nature of the transparent reactance from capacitive to inductive, which could lead to the excitation of a higher order (TE-dominant) SW mode.

Adiabatic Floquet Wave Expansion

One of the main properties of the *constant-average* reactance $\underline{\underline{\mathbf{X}}}$ in (2) is related to the fact that the *average* current flowing in it is quite similar to the SW-current that the dipole source would excite in $\underline{\underline{\mathbf{X}}}^{(0)}$. An appropriate modification - illustrated next - of these currents will constitute therefore the 0-index mode of an adiabatic FW expansion. Since $\underline{\underline{\mathbf{X}}}^{(0)}$ is $\boldsymbol{\rho}$-independent, the SW that flows on it, excited by a dipole, is a purely TM cylindrical wave asymptotically given by

$$\mathbf{J}_0 = J_0 H_1^{(2)}(\beta_{sw}\rho)\,\hat{\boldsymbol{\rho}} \tag{5}$$

where $H_1^{(2)}$ is the Hankel function of second kind and first order. The propagation constant β_{sw} is solution of a dispersion equation affected by the $\overline{X}_\rho$ component only, and it is given as a function of the scalar opaque reactance $\overline{X}_{op}$ as $\beta_{sw} = k\sqrt{1 + \overline{X}_{op}^2/\zeta^2}$. An excellent closed-form approximation of β_{sw} can be found in [11].

In presence of the modulation, the 0-indexed FW mode (simply denoted hereinafter as "0-mode") is obtained from (5) by *locally* transforming the real unperturbed wavenumber β_{sw} into the complex radial wavenumber $k^{(0)}(\boldsymbol{\rho}) = \beta_{sw} + \beta_\Delta(\boldsymbol{\rho}) - j\alpha(\boldsymbol{\rho})$. It is therefore implicitly assumed that the 0-mode has a cylindrical wavefront with radial attenuation with *local* attenuation parameter $\alpha(\boldsymbol{\rho})$ accounting for the transfer of energy from the 0-mode to the leaky mode along the propagation path. The parameters $\beta_\Delta(\boldsymbol{\rho})$ and $\alpha(\boldsymbol{\rho})$ are functions of the $\underline{\underline{\mathbf{X}}}$ entries. Since $k^{(0)}(\boldsymbol{\rho})$ is space-dependent, its associated *global* phase $\tilde{k}^{(0)}(\boldsymbol{\rho})\rho$ from the reference point in the origin is obtained by integrating the local relation

$\partial\left(\tilde{k}^{(0)}(\boldsymbol{\rho})\rho\right)/\partial\rho = k_0(\boldsymbol{\rho})$. This leads to the adiabatic FW expansion for the current $\mathbf{J} \approx \sum_n \mathbf{J}^{(n)}$, with

$$\mathbf{J}^{(n)} = \left(J_\varphi^{(n)}\hat{\boldsymbol{\varphi}} + J_\rho^{(n)}\hat{\boldsymbol{\rho}}\right) e^{-jnKs(\boldsymbol{\rho})} H_1^{(2)}\left(\tilde{k}^{(0)}\rho\right) \tag{6}$$

and where $Ks(\boldsymbol{\rho})$ is the same as in (4). Taking the asymptotic form of the Hankel function, it is evident that each mode in (6) has a curvilinear-wavefront which propagates with *local* n-indexed FW wavevectors

$$\boldsymbol{\beta}^{(n)} = \mathrm{Re}\nabla_t\left[\tilde{k}^{(0)}\rho + nKs(\boldsymbol{\rho})\right] = (\beta_{sw} + \beta_\Delta)\,\hat{\boldsymbol{\rho}} + nK\nabla_t s(\boldsymbol{\rho}) \tag{7}$$

and with n-independent local attenuation parameter $\alpha(\boldsymbol{\rho})$. The curvilinear wavefront associated with each FW current mode is given by $\beta_{sw}\rho + nKs(\boldsymbol{\rho}) = const$. The adiabatic FW electric fields expansion can be obtained by the spectral Green's function (GF) $\underline{\underline{\mathbf{Z}}}_{GF}^{(n)}$ of the grounded slab evaluated at the local wavevectors $\boldsymbol{\beta}^{(n)}$ (see appendix in [7]), that is

$$\mathbf{E}_t(\boldsymbol{\rho}) = \sum_n \mathbf{E}^{(n)} \approx \sum_n \underline{\underline{\mathbf{Z}}}_{GF}^{(n)} \cdot \mathbf{J}^{(n)} \tag{8}$$

We point out that the basis on which we have expanded currents and fields does not rigorously satisfy Maxwell's equations, since it is based on an asymptotic, adiabatic approximation valid far from the point source. However, this basis locally recovers a FW expansion and may be used for obtaining an adiabatic solution. This solution is found by using (8) in the transparent IBCs (1) leading to

$$\sum_n \underline{\underline{\mathbf{Z}}}_{GF}^{(n)} \cdot \mathbf{J}^{(n)} = \sum_n j\underline{\underline{\mathbf{X}}} \cdot \mathbf{J}^{(n)} \tag{9}$$

and allowing one to find an analytical solution and a local $\boldsymbol{\rho}$–dependent adiabatic dispersion equation. To this end, the terms in (9) with the same rapid phase variation are equated and a set of equations is obtained. The set is solved by substitutions, leading to an homogeneous system of type $j\underline{\underline{\chi}}(\boldsymbol{\rho}) \cdot \mathbf{J}^{(0)} = 0$ that admits a non-trivial solution only for $\det[\underline{\underline{\chi}}(\boldsymbol{\rho})] = 0$. This identifies the *local dispersion equation* whose solution gives the complex value of the 0-mode *local* wavenumber $k^{(0)}$.

3. Design of Modulated MTS Antennas

The global synthesis scheme is shown in Fig. 2 [8] and it is composed of three main blocks. The first block synthesizes the continuous impedance surface, which produces the objective aperture field when excited by a reference SW. Then, within the second block, the continuous impedance surface is discretized and implemented through a dense texture of small patches (typically several thousands). Finally, the third block analyses the textured antenna layout through a global full-wave solver.

The design process starts assuming that the radiative components of the objective aperture field are known. In the first block, the synthesis of the IBCs is performed representing the patterned metallic cladding by a continuous,

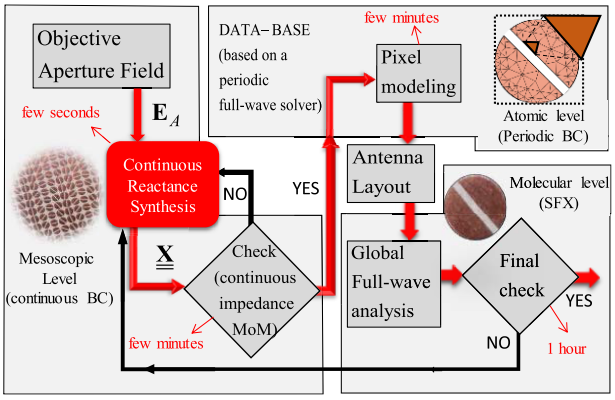

Fig. 2 Block diagram of the synthesis process [8].

space-dependent reactance tensor $\underline{\underline{\mathbf{X}}}$, which models the continuous anisotropic IBC related to the discontinuity of the magnetic field. The red block is the core of this task and it is based on the analytical FO method detailed in [7], [8].

After the synthesis has been performed, a full wave analysis, still based on the continuous IBC approach, is used to check the accuracy of the synthesized reactance. This step is performed with the extremely fast formulation detailed in [12]. If the first check with this solver is successful, one proceeds to the implementation of the obtained IBC by means of sub-wavelength patches.

Notice that the synthesis procedure could be also extended to different impedance implementation (e.g. fully metallic elements) by considering impenetrable impedances instead of penetrable ones.

The element synthesis ("pixel modelling" in Fig. 2) is carried out using a local "micro-periodicity" concept, i.e., assuming that the local element is immersed in a periodic environment of identical elements with the periodicity of the lattice. The above assumption allows one to apply periodic IBCs on the elemental cell boundaries and to use the periodic GF in the integral equation formulation, thus reducing the computational effort to that of a single unit cell. The analysis of the periodic structure, which is inherently extremely fast, is repeated several times in order to construct a database. Such a database associates to different element geometries, within the unit cell, the corresponding entries of the anisotropic reactance tensor. The database can be built before the entire synthesis process, and possibly reused for other syntheses. Actually, only a few samples of the parameter-space are directly calculated and an interpolation is next used to create a denser database. The database is normally constructed at the antenna operative frequency; its extension around the operative frequency can be important when the antenna is required to operate over a large band. To this purpose, the pole-zero matching method [13] or the analytical models presented in [11] and [14] can be used. The output of this part of the design is a complete layout of the antenna, where the dimensions and the orientation of any single pixel-element are defined.

The final phase of the design process is a detailed analy-

sis of the pixelated layout, which requires a global full-wave solver. In case the final check is not successful, a repetition of the continuous model synthesis may be required. Actually, as the analytic core of the synthesis, i.e. the "continuous reactance synthesis" block in Fig. 2, is powerful and accurate, the overall process rarely requires a feedback. This might be needed for very demanding requirements, like a large bandwidth or a very high efficiency.

4. Efficiency of MTS Antennas

Efficiency is defined here as the ratio between the gain of the antenna and the maximum directivity of an ideal, lossless, uniformly illuminated aperture having the same area. The characterization of the efficiency for MTS antennas involves several aspects related to the radiation mechanism [15] which are sketched in Fig. 3. When the input port of the feeder is fed by a power P_{in}, part of it is directly radiated in free space (P_{feed}), while the remaining power is transformed into a SW (P_{sw}). The SW power is partly lost due to losses (P_Ω), partly radiated as a LW (P_{lw}), and the remaining part reaches the antenna rim, giving rise to edge effects: diffraction (P_{diff}) and reflection, giving rise to an inward SW (P_{swb}). In practical designs, P_{swb} is negligible and one may assume that all the reflected power is fully reradiated (P_{lwb}). All the phenomena relevant to the introduced wave-mechanism are characterized through the definitions of relevant efficiencies that will be discussed in the following.

Feed Efficiency

The feed efficiency ε_{feed} is defined as the ratio between the input power and the power delivered to the SW, i.e.

$$\varepsilon_{feed} = P_{sw}/P_{in} = 1 - P_{feed}/P_{in} \tag{10}$$

Ideally, the feeder of a MTS antenna delivers all the input power to the SW but a real feeder will always have a residual P_{feed}, directly radiated in free space. The problem of the optimum excitation of surface waves for this kind of antennas is detailed in [15].

Ohmic efficiency

To define the ohmic efficiency we assume lossless metals and a lossy substrate, which is reasonable in the microwave regime where the dielectric losses dominate on the metal losses. The ohmic efficiency ε_Ω is defined as

$$\varepsilon_\Omega = \frac{P_{lw}/P_{sw}}{P_{lw}|_{P_\Omega=0}/P_{sw}} \tag{11}$$

which stands for the ratio between the radiated power P_{lw} and the SW power P_{sw} in presence of losses and the same ratio in absence of losses ($P_{lw}|_{P_\Omega=0}$ is the LW power in absence of losses). In presence of ohmic-losses the propagation constant β_{sw} on a non-modulated MTS becomes slightly complex, namely $\beta_{sw} \to \overline{\beta}_{sw} = \beta_{sw} - j\alpha_p$, with the phase parameter β_{sw} not significantly affected. The attenuation constant α_p can be estimated by solving the dispersion equation with a perturbative approach [15].

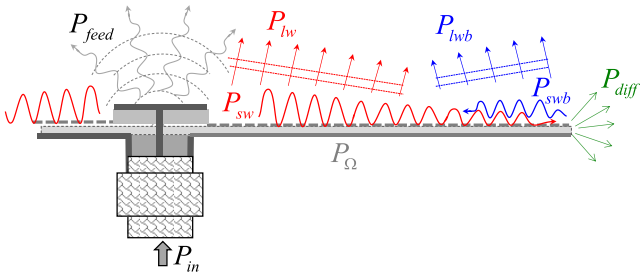

Fig. 3 Visualization of the time average power contributions for the characterization of the antenna efficiency.

Conversion and Tapering efficiency

Conversion efficiency represents the fraction of radiated LW power with respect to the SW power. In absence of losses, i.e. when $P_\Omega = 0$, the conversion efficiency ε_{conv} is

$$\varepsilon_{conv} = P_{lw}|_{P_\Omega=0}/P_{sw} \tag{12}$$

The tapering efficiency ε_{tap} is related to the directivity loss of a given aperture illumination with respect to a uniform distribution. For broadside beams, it is quantified as

$$\varepsilon_{tap} = \frac{\left|\iint_A \mathbf{E}_t\, dA\right|^2}{A\iint_A |\mathbf{E}_t|^2\, dA} = \frac{\left|\iint_A \sqrt{S(\rho)}dA\right|^2}{A\iint_A S(\rho)dA} \tag{13}$$

where $\mathbf{E}_t$ is the aperture field distribution and $S(\rho)$ is the power density distribution associated with $\mathbf{E}_t$. The right-hand side of (13) comes from the relation $E_t \approx \sqrt{2\zeta S(\rho)}$ valid for broadside beam antennas. The quantities in (12) and (13) are controlled by the attenuation parameter α, which is controlled by the amplitude of the modulation [8].

Overall Efficiency

Figure 4 shows a plot of the overall efficiency for broadside, circularly polarized MTS antennas with different sizes, given by the product of all the efficiencies introduced. We have assumed a feeder formed as a vertical electric dipole on top of a circular patch printed on the MTS, designed to maximize the SW power (see inset of Fig. 4). Two different standard lossy substrates have been considered with $\varepsilon_r = 9.8$ and $\varepsilon_r = 4.5$, respectively, with identical dissipation factor $\tan\delta = 0.002$. The power distribution on the aperture is

$$\frac{S(\rho_\lambda)}{S_{\max}} = \begin{cases} \sin^2(\pi\rho_\lambda); & \rho_\lambda \le 0.5 \\ 1; & 0.5 < \rho_\lambda \le a_\lambda - 2 \\ \sin^2\left[\frac{\pi}{4}(a_\lambda - \rho_\lambda)\right]; & a_\lambda - 2 < \rho_\lambda \le a_\lambda \end{cases} \tag{14}$$

so that tapering and conversion efficiencies approximately follow the relation $\varepsilon_{conv} = \varepsilon_{tap} = \sqrt{a_\lambda/(a_\lambda+2)}$, where a_λ is the aperture radius normalized to λ. Figure 5 shows an example of the directive pattern radiated by the distribution in (14) when $a_\lambda = 8$ and predicted by the full-wave solver for continuous IBCs [12]: peak directivity is around 33.3 dBi,

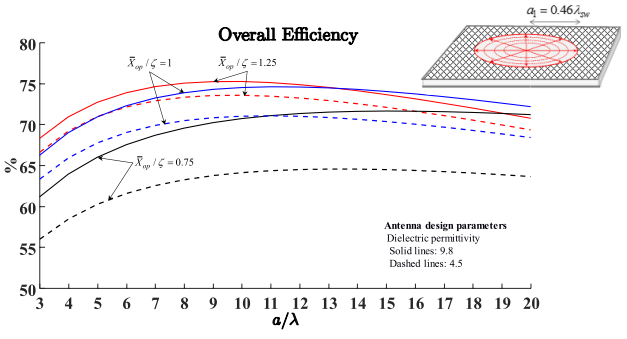

Fig. 4 Overall efficiency for broadside circularly polarized MTS antennas with several sizes and several values of the normalized opaque impedance $\bar{X}_{op}/\zeta$. Curves are for substrates with $h = 0.2/k$ and loss tangent of 0.002.

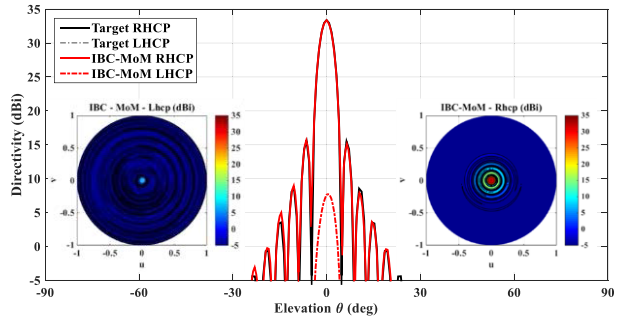

Fig. 5 Directive pattern from a MTS with high tapering efficiency. Red lines: IBC-MoM [12]. Black lines: target directivity patterns. Solid lines: RHCP; dotted-dashed lines: LHCP. Insets: directive diagrams in the u-v spectral plane from the IBC-MoM.

corresponding to a tapering efficiency of about 85%. The MTS structure is designed for $\overline{X}_{op} \approx 0.9\zeta$, on a substrate with $h = 0.2/k$ and $\varepsilon_r = 9.8$, is fed by an elementary vertical dipole and the aperture field distribution is such that x and y components are in phase quadrature to radiate a right hand circularly polarized field.

The overall efficiency is plotted in Fig. 4 for several values of the opaque impedance that can be implemented with printed patches. It is seen that the overall efficiency can reach 75% with a design that makes use of standard substrates, a non-uniform modulation and a simple feeder. The values in Fig. 4 are typical overall efficiency figures and can be improved under specific conditions. On the other side, additional requirements on the antenna pattern, e.g. a need of low side lobes or cross-polar radiation, may adversely affect the efficiency like for any other antenna topology.

5. Bandwidth of Gain

Here the antenna bandwidth is the frequency range in which the gain is larger than −3 dB with respect to the gain at the design frequency. The rate at which the antenna loses gain when changing frequency is related to the dispersion of the MTS [16]. In fact, this dispersion introduces a variation $\beta_{sw} \rightarrow \beta_{sw} + \Delta\beta_{sw}$ and $\alpha \rightarrow \alpha + \Delta\alpha$ implying a phase mismatch between the SW-wavenumber and $Ks(\boldsymbol{\rho})$, as well as a distortion of the amplitude of the aperture field. The main detrimental effect on the gain is due to the phase error; this affects the matching between the modulation phase function $Ks(\boldsymbol{\rho})$ and the SW phasing $\beta_{sw}(\omega)\rho$ of a quantity proportional to the integral of $\beta_\Delta(\omega, \rho)$ along the SW path [7], [8]. Therefore, only the effect of $\Delta\beta_{sw}$ will be considered hereinafter. The value of $\Delta\beta_{sw}$ is obtained by the first order Taylor expansion of $\beta_{sw}(\omega)$ at the center frequency, i.e.

$$\Delta\beta_{sw} \approx \Delta\omega \cdot (\partial\beta_{sw}/\partial\omega) = \Delta\omega/v_g \tag{15}$$

where v_g is the group velocity of the SW at the center frequency and $\Delta\omega$ is the unilateral angular-frequency bandwidth. The antenna gain is defined as

$$G = (ka)^2\varepsilon \tag{16}$$

where $(ka)^2$ is the directivity of a uniformly illuminated circular aperture of radius a and ε is the antenna efficiency. From (16), the reduction of gain with frequency is translated into a decrease of the antenna efficiency. Naming ε the efficiency at the design working frequency, and ε' the efficiency when a shift $\Delta\beta_{sw}$ arises on the wavenumber due to the frequency change, the unilateral bandwidth is obtained when the condition $\varepsilon' = 0.5\varepsilon$ is met.

Bandwidth of a highly efficient MTS antenna

We discuss here the bandwidth of a highly efficient MTS antenna radiating a broadside beam. On the antenna surface, we consider the power distribution given in (14), which provides a good tapering efficiency. We also assume that the major contribution to the reduction of ε comes from the reduction of the tapering efficiency ε_{tap}, which is coherent with the premise that the phase error is the main detrimental effect on the gain. The unilateral bandwidth is given therefore by the condition:

$$\left|\int_0^a \sqrt{S(\rho)}e^{-j\Delta\beta_{sw}\rho}\rho d\rho\right|^2 = \frac{1}{2}\left|\int_0^a \sqrt{S(\rho)}\rho d\rho\right|^2 \tag{17}$$

To estimate the antenna bandwidth, we use (14) into (17) and solve this latter numerically for finding $\Delta\beta_{sw}$. The numerical solution is well approximated by $\Delta\beta_{sw} \approx 3.77/a$. Using the latter expression in (15) gives a bilateral *relative* bandwidth

$$B = 2\frac{\Delta\omega}{\omega} \approx 1.2\gamma\frac{1}{a_\lambda} < 1.2\frac{1}{a_\lambda} \tag{18}$$

where $\gamma = v_g/c$ is the group velocity normalized to the speed of light c in free space. Figure 6 summarizes efficiency and bandwidth of broadside MTS antennas as a function of the antenna radius, for several values of the opaque impedance. The results in Fig. 6 have been obtained for a lossless substrate with permittivity $\varepsilon_r = 10$ and thickness $h = 0.2/k$. Efficiency plots assume a feed efficiency as the one of a vertical electric dipole with a metallic disc printed on the MTS

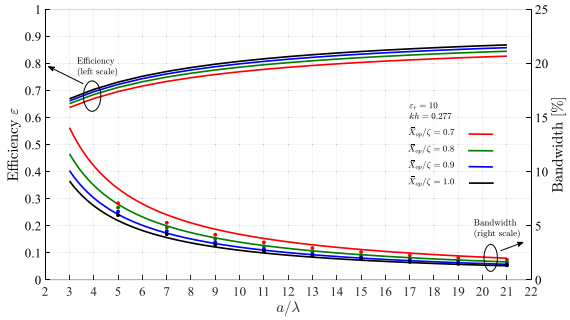

Fig. 6 Efficiency and bandwidth plots of a broadside MTS antenna, realized on a lossless substrate with $\varepsilon_r = 10$, $h = 0.2/k$, and implementing the power distribution in (14). The MTS is assumed fed by vertical electric dipole on an annular patch. Circular dots come from the FO analysis [7].

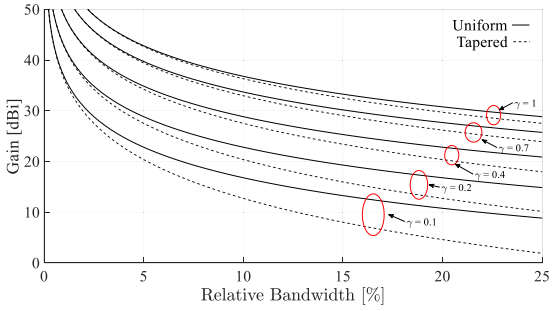

Fig. 7 Gain as a function of relative bandwidth for the tapered distribution in (14) and a uniform amplitude distribution, for several values of $\gamma = v_g/c$.

(as in Fig. 4). One can conclude, from Fig. 6, that higher values of the opaque impedance increase the antenna efficiency at the cost of a smaller bandwidth.

A representation useful in practice relates the antenna gain in dBi for $\varepsilon_{feed}\varepsilon_{tap} = 1$ to the percentage bandwidth $B_{\%}$. To this purpose, we evaluate the product between the antenna gain in (16) and the half-power relative bandwidth in (18) when $\varepsilon_{feed}\varepsilon_{\Omega} = 1$ and $\varepsilon_{conv}\varepsilon_{tap} = a_\lambda/(a_\lambda + 2)$, obtaining:

$$GB \approx 47.37\gamma \frac{a_\lambda}{(a_\lambda + 2)} a_\lambda < 47.37 a_\lambda \tag{19}$$

where the term into square brackets can be approximated to unity for large a_λ. Using again Eq. (18) and taking the logarithm leads to:

$$G[dB] \approx 57 - 10\log\left(1 + \frac{1}{60}\frac{B_{\%}}{\gamma}\right) - 20\log\left(\frac{B_{\%}}{\gamma}\right) \tag{20}$$

Figure 7 plots (20) as function of the percentage bandwidth for γ ranging from 0.3 to 1. Also, the same picture shows the theoretical bandwidth of a MTS antenna having a uniform illumination. Although this case is not physically feasible, it is useful as a theoretical limit for the bandwidth of a MTS antenna designed to maximize the antenna efficiency.

Enlarging the bandwidth of modulated MTS Antennas

A proper design approach for a wideband MTS aperture should implement a *local compensation* for the SW wavelength frequency variation by a radial shaping of the modulation phase $Ks(\boldsymbol{\rho})$. For this reason an optimal design of $Ks(\boldsymbol{\rho})$ relies on the frequency characterization of the cladding reactance $\underline{\underline{\mathbf{X}}}(\boldsymbol{\rho}, \omega)$ on the band of interest; anyway, usually, the frequency variation of this latter is of a second order effect w.r.t. the slab contribution and a quite good characterization can be provided by assuming a linear function of the frequency, at least in a certain range of frequency [11]. The shape chosen for $Ks(\boldsymbol{\rho})$ can be expressed by $Ks(\rho) = 2\pi\rho/f_p(\rho)$, where

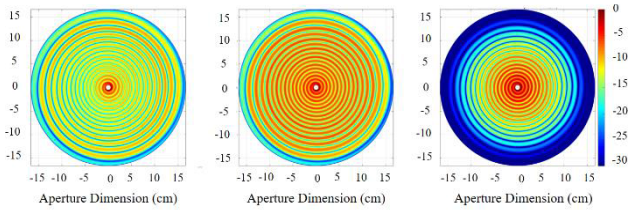

Fig. 8 Representation of induced currents on wideband aperture: (a) at a frequency of 18.33 GHz, (b) at a frequency sample of 23.94 GHz and (c) at 29.88 GHz. It is shown how aperture activation changes over the band. As the operating frequency shifts to high, illumination is less homogeneous and more confined at inner region where most of the SW power is radiated away. Conversely at lower frequencies SW power reaches outer region where a broadside beam is generated.

$$f_p = (d_1 - \xi) + \xi \sum_{i=0}^{\infty} \frac{(\delta\rho)^i}{i!} \tag{21}$$

with $\delta = \ln\left[(d_2 - d_1)/\xi - 1\right]/a$ and ξ is a constant parameter. Hence modulation period reads $p(\rho) = f_p^2/\left(f_p - \rho\xi\delta e^{\delta\rho}\right)$ and for small ξ assumes a quasi-exponential shape. This setting of the modulation periodicity realizes a local matching between the wavelength of the SW and a certain annular region of the aperture. Changing the frequency, this region slides in or out on the aperture matching a different region of impedance. Namely, the mechanism becomes an active region mechanism. Within the active region the SW is transformed into a LW that radiates a beam in the desired direction being its phase evolution locally matched to the modulation phase, leading to broadside radiation. In other annular aperture regions, only weak radiation occurs, due to the phase mismatch which does not allow the SW-MTS interference field to enter into the visible range. Induced aperture fields at three frequency samples are plotted in Fig. 8.

The values of d_1, d_2 are chosen to match the modulation phase to the SW phase progression at the two band extremes, according to the relation $2\pi/p_{1,2} = \beta_{sw}(f_{1,2})$, where $p_1 = p|_{\rho=0}$, $p_2 = p|_{\rho=a}$, $f_{1,2}$ are the limit operating frequencies and β_{sw} is related to the opaque average MTS impedance.

The aperture example treated in this section operates at K and Ka band in a frequency range comprised between 18 GHz and 30 GHz.

The radius of the antenna is fixed as $a = 16.66\,\text{cm}$, the substrate on which the MTS is synthesized is a Rogers RO3006 featuring a permittivity $\varepsilon_r = 6.15$ and thickness $h = 0.635\,mm$.

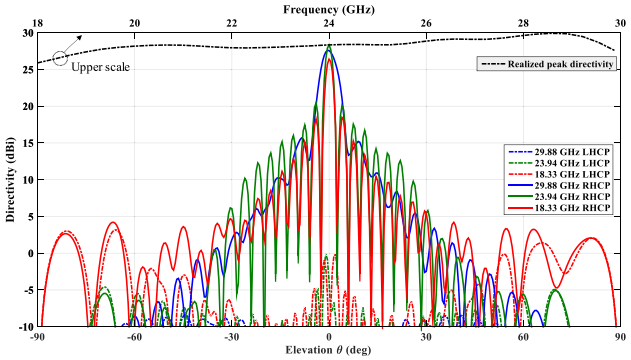

Fig. 9 Directive patterns for a broadband modulated MTS antenna obtained from a continuous impedance boundary conditions (IBC) MoM solver [12]. Cuts along the $v = 0$ spectral line are shown. In the same frame, it is reported the peak directivity (top scale) which has a good stability within the K and Ka-band in the range 18–30 GHz.

The design frequency of the MTS impedance is fixed at 27 GHz; at that frequency the MTS is characterized by an average transparent reactance $\overline{X}_{\rho,\phi} = -450\,\Omega$ (as expressed in (4)). This reactance value is considered linear on the overall desired bandwidth (from 18 GHz to 30 GHz in this example). Values for d_1 and d_2 are hence determined and are respectively equal to 0.72 and 1 whereas ξ equals to 0.06 for the present case.

A single centered TM launcher constituted by a vertical electric dipole embedded into the substrate feeds the structure; the antenna in-band response is calculated by the use of a MoM tool presented in [12]. The calculated directivity patterns are shown in Fig. 9 for a set of three frequency samples together with the aperture frequency response. We observe in Fig. 9 an extremely flat aperture response in terms of the calculated directivity and good in-band pattern shape stability; broadside pointing is maintained within the band of interest and excellent polarization purity is also displayed at the three frequency samples.

The design method presented here proves to be an efficient way to trade the available aperture and hence efficiency (that is around the 10% within the band in this example) for a wideband operability by progressive activation of the different antenna functional regions in much the same way as it happens in spiral and log-periodic antennas. Thus, as a matter of fact, the example serves to demonstrate that typical LWAs frequency beam squinting can be overcomed by proper MTS IBCs design. As a result, bandwidth improvement is obtained w.r.t. to more classical MTS antenna solutions and achieved relative bandwidth is close to $B_{\%} \approx 50\%$.

6. Concluding Remarks

Modulated MTS antennas are a significant improvement from traditional antenna solutions. Rather than shaping a fixed boundary condition (mostly PEC) to achieve the desired radiation characteristics, they offer the possibility to design the boundary condition itself to achieve the desired behaviour. The full control of the aperture field and hence of the far field properties (beam shape, polarization, efficiency, bandwidth) is strictly related to the capability of accurately designing the MTS. Here, we have provided a summary of the analysis method and design process of MTS antennas and a global picture of their performance in terms of efficiency and bandwidth.

References

[1] G. Minatti, M. Faenzi, E. Martini, F. Caminita, P. De Vita, D. Gonzalez-Ovejero, M. Sabbadini, and S. Maci, "Modulated metasurface antennas for space: Synthesis, analysis and realizations," IEEE Trans. Antennas Propag., vol.63, no.4, pp.1288–1300, April 2015.

[2] A.M. Patel and A. Grbic, "A printed leaky-wave antenna based on a sinusoidally-modulated reactance surface," IEEE Trans. Antennas Propag., vol.59, no.6, pp.2087–2096, June 2011.

[3] B.H. Fong, J.S. Colburn, J.J. Ottusch, J. L Visher, and D.F. Sievenpiper, "Scalar and tensor holographic artificial impedance surfaces" IEEE Trans. Antennas Propag., vol.58, no.10, pp.3212–3221, Oct. 2010.

[4] M. Faenzi, F. Caminita, E. Martini, P. De Vita, G. Minatti, M. Sabbadini, and S. Maci, "Realization and measurement of broadside beam modulated metasurface antennas," IEEE Antennas Wireless Propag. Lett., vol.15, pp.610–613, 2016.

[5] S. Pandi, C.A. Balanis, and C.R. Birtcher, "Design of scalar impedance holographic metasurfaces for antenna beam formation with desired polarization," IEEE Trans. Antennas Propag., vol.63, no.7, pp.3016–3024, July 2015.

[6] D. González-Ovejero, T.J. Reck, C.D. Jung-Kubiak, M. Alonso-DelPino, and G. Chattopadhyay, "A class of silicon micromachined metasurface for the design of high-gain terahertz antennas," IEEE Int. Symp. Antennas Propag. (APSURSI), pp.1191–1192, Fajardo, 2016.

[7] G. Minatti, F. Caminita, E. Martini, and S. Maci, "Flat optics for leaky-waves on modulated metasurfaces: Adiabatic Floquet-wave analysis," IEEE Trans. Antennas Propag., vol.64, no.9, pp.3896–3906, Sept. 2016.

[8] G. Minatti, F. Caminita, E. Martini, M. Sabbadini, and S. Maci, "Synthesis of modulated-metasurface antennas with amplitude, phase and polarization control," IEEE Trans. Antennas Propag., vol.64, no.9, pp.3907–3919, Sept. 2016.

[9] M.A. Francavilla, E. Martini, S. Maci, and G. Vecchi, "On the numerical simulation of metasurfaces with impedance boundary condition integral equations," IEEE Trans. Antennas Propag., vol.63, no.5, pp.2153–2161, May 2015.

[10] E. Martini, M. Mencagli, Jr., and S. Maci, "Metasurface transformation for surface wave control," Philos. Trans. R. Soc. A, vol.373, no.2049, p.20140355, 2015.

[11] M.J. Mencagli, E. Martini, and S. Maci, "Transition functions for closed form representation of metasurface reactance," IEEE Trans. Antennas Propag., vol.64, no.1, pp.136–145, Jan. 2016.

[12] D. Gonzalez-Ovejero and S. Maci, "Gaussian ring basis functions for the analysis of modulated metasurface antennas," IEEE Trans. Antennas Propag., vol.63, no.9, pp.3982–3993, Sept. 2015.

[13] S. Maci, M. Caiazzo, A. Cucini, and M. Casaletti, "A pole-zero matching method for EBG surfaces composed of a dipole FSS printed on a grounded dielectric slab," IEEE Trans. Antennas Propag., vol.53, no.1, pp.70–81, Jan. 2005.

[14] M.J. Mencagli, C. Della Giovampaola, and S. Maci, "A closed-form representation of isofrequency dispersion curve and group velocity for surface waves supported by anisotropic and spatially dispersive metasurfaces," IEEE Trans. Antennas Propag., vol.64, no.6, pp.2319–2327, June 2016.

[15] G. Minatti, E. Martini, and S. Maci, "Efficiency of metasurface antennas" IEEE Trans. Antennas Propag., vol.65, no.4, pp.1532–

1541, April 2017.
[16] G. Minatti, M. Faenzi, M. Sabbadini, and S. Maci, "Bandwidth of gain in metasurface antennas," IEEE Trans. Antennas Propag., vol.65, no.6, pp.2836–2842, June 2017.

Marco Faenzi was born in Siena, Italy. He received the Master degree in telecommunication engineering (with a score of 110/110) from the Department of Information Engineering and Mathematical Science at University of Siena, Siena, Italy, in 2011. In the same year he won a Ph.D. position at the Department of Information Engineering and Mathematical Sciences focused on the development of high gain apertures based on modulated metasurface structures exploiting inductive and capacitive textures. He successively gained the Ph.D. degree in 2015. In 2015 he won a Post-Doc grant co-financed by European Space Agency and University of Siena. He has worked on metasurfaces holographic patterning for the optimization of aperture efficiency of dipoles excited planar resonator. During the Post-Doc activity he worked towards characterization and synthesis of modulated metasurface apertures capable of multiband and broadband operativity.

Gabriele Minatti was born in Florence, Italy. He received the MSc degree (cum laude) in Electronic Engineering from the University of Florence in 2008 and the Ph.D. degree from University of Siena in 2012. From October 2012 to September 2014 he has been with the European Space Agency, antennas and sub-millimeter waves section, in the post of internal research fellow. From 2015 to 2017 he has been with the University of Siena in the post of research assistant, mainly working on modelling, analysis and design of metasurface antennas. He is presently an antenna engineer with Wave-Up S.r.l, Florence, Italy. Dr. Minatti was co-recipient of the Best Paper Award on Antenna Theory Award at the 5th European Conference on Antennas and propagation (EuCAP, Rome, Italy, 2011), the Antenna Innovation Award at the 33rd ESA Antenna Workshop (ESTEC, Noordwijk, The Netherlands, 2011), the student paper contest at 17th International Symposium on Antennas and Propagation (ISAP, Nagoya, Japan, 2012). In 2016, he was co-recipient of the IEEE Schelkunoff Prize Paper Award, and in 2017 of the Best Paper Award in Antenna Design and Application at the 11th European Conference on Antennas and Propagation (EuCAP, Paris, France, 2017).

Stefano Maci (IEEE F 2004) received the Laurea Degree cum Laude at University of Florence in 87 and from '97 is a Professor at the University of Siena. His research interest includes high-frequency and beam representation methods, computational electromagnetics, large phased arrays, planar antennas, reflector antennas and feeds, metamaterials and metasurfaces. Since 2000 he was member the Technical Advisory Board of 11 international conferences, member of the Review Board of 6 International Journals. He organized 25 special sessions in international conferences, and he held 10 short courses in the IEEE Antennas and Propagation Society (AP-S) Symposia about metamaterials, antennas and computational electromagnetics. In 2004–2007 he was WP leader of the Antenna Center of Excellence (ACE, FP6-EU) and in 2007–2010 he was International Coordinator of a 24-institution consortium of a Marie Curie Action (FP6). He has been Principal Investigator from 2010 of 6 cooperative projects financed by European Space Agency. In 2004 he was the founder of the European School of Antennas (ESoA), a post graduate school that presently comprises 30 courses on Antennas, Propagation, Electromagnetic Theory, and Computational Electromagnetics and 150 teachers coming from 15 countries. Stefano Maci has been a former member of the AdCom of IEEE Antennas and Propagation Society (AP-S), associate editor of AP-Transaction, Chair of the Award Committee of IEEE AP-S, and member of the Board of Directors of the European Association on Antennas and Propagation (EurAAP). He has been former member of the Antennas and Propagation Executive Board of the Institution of Engineering and Technology (IET, UK). He is the director of the consortium FORESEEN, presently involving 40 European Institutions. He was co-founder of 2 Spin-off Company. He was a Distinguished Lecturer of the IEEE Antennas and Propagation Society (AP-S) in 2010–14, and recipient of the EurAAP Award in 2014, the IEEE Schelkunoff Transaction Prize 2016, and the Chen-To Tai Distinguished Educator award 2016. His research activity is documented in 140 papers published in international journals, (among which 90 on IEEE journals), 10 book chapters, and about 300 papers in proceedings of international. These papers have received around 4900 citations.